Eur. Phys. J. D **13**, 207–212 (2001)

THE EUROPEAN PHYSICAL JOURNAL D

EDP Sciences

Interpretation of the structures observed for excitation cross-sections in C^{2+}/He^{2+}–Li collisions

A. Dubois[1,a] and J.P. Hansen[2]

[1] Laboratoire de Chimie Physique-Matière et Rayonnement[b], Université Pierre et Marie Curie, 11 rue Pierre et Marie Curie, 75231 Paris Cedex 05, France
[2] Institute of Physics, University of Bergen, Allégaten 55, 5007 Bergen, Norway

Received 7 July 2000

Abstract. The existence of oscillatory or plateau like structures in the low energy dependence of the excitation cross-sections in ion-atom collisions has recently been subject of different interpretations based on model calculations. We report atomic-state close-coupling calculations for the description of $Li(2s \rightarrow 2p)$ excitation by He^{2+} and C^{2+} impact where the appearance of such structures is very different and previously documented in experimental studies. A system specific interpretation based on *dynamic* adiabatic energy curves is given and the interplay between high-energy direct and low-energy molecular mechanisms in the two systems are discussed.

PACS. 34.10.+x General theories and models of atomic and molecular collisions and interactions (including statistical theories, transition state, stochastic and trajectory models, etc.) – 34.50.Fa Electronic excitation and ionization of atoms (including beam-foil excitation and ionization) – 34.50.Pi State-to-state scattering analyses

1 Introduction

Perturbative approaches to describe excitation in ion-atom collisions give rise to *bell-shape* behaviour of the related cross-sections *versus* impact energy. This feature, which in this case stems from a stationary phase argument, is also present at intermediate energies when close-coupling is required and is connected to a dominant direct, state-to-state, mechanism. In a semi-classical interpretation, this usually takes place at large internuclear distances and involves the characteristics of the separated atomic states and of the interaction responsible, essentially Coulombic. In a classical picture, this has also been interpreted by a mechanism in which the active electron has exactly time enough to change its energy, staying located around the target. Recently, this mechanism has been baptised in terms of the number of times a classical electron crosses the mid-plane separating the two nuclei; direct excitation then corresponds to the so-called *no-swap* process [1,2].

For decreasing impact energies the excitation cross-sections drop off rapidly, but generally not monotonously, and present shoulders, plateaus or oscillations, however smaller in magnitude than the direct mechanism peak. These features have been explained in terms of small internuclear distance two-centre mechanisms, involving the molecular characteristics of the transient diatomic complex [3,4]. The classical equivalence is the *sharing* of the active electron which may be temporarily delocalized on one or the other collision partner, *cf.* the *multi-swap* interpretation of excitation [2]. Note that in the framework of classical mechanics this transient diatomic structure has no relation and common characteristics with a molecule.

A study of these oscillations for $H(1s \rightarrow n = 2)$ excitation induced by He^{2+} impact has been performed based on the *hidden-crossings* theory [5]. This low-energy model involves the impact velocity in the standard expression of the transition probabilities at crossings and in the phases responsible of the interference, but not in the distorted electronic structure of the transient molecule.

On the other hand, during the collision, the motion of the projectile states with respect to the target centre has major consequences onto the probabilities for the different open channels to occur. Indeed the space-fixed projectile orbitals cannot be considered as eigenfunctions of the isolated moving atom: this fact is expressed by the multiplication of the projectile orbitals by phase factors taking into account this translation. The more straightforward phase is the plane-wave Electronic Translation Factor (ETF) used in the atomic-state close-coupling model [6], *i.e.* $e^{i\mathbf{v}.\mathbf{r}-i\frac{1}{2}v^2}$, where $\mathbf{v}$ is the relative impact velocity. In addition to the distortion of the states, this implies the

[a] e-mail: ad@ccr.jussieu.fr
[b] Unité mixte de recherches du CNRS, UMR 7614.

shift of their energies by the corresponding kinetic energy term included in the ETF phases. In singly-charged ion-atom collisions, for example, the effects of these phases have been recently discussed and verified experimentally in relation with orientation effects occurring for near-resonant electron capture channels [7,8].

In this paper we present an interpretation of the presence of different plateaus in Li($2s \to 2p$) excitation cross-sections for two similar doubly charged projectiles, He^{2+} and C^{2+}. The results are based on an atomic-state close-coupling semi-classical model. We used a minimal basis set which results agree with those obtained recently experimentally and by large basis coupled-channel calculations [9,10]. The differences between the two systems in the location and appearance of the plateaus are discussed in terms of molecular energy curves and avoided crossings obtained by diagonalisation of the electronic Hamiltonian on our minimal diabatic basis.

Atomic units are used unless otherwise stated.

2 Theoretical method

2.1 The semi-classical close-coupling model

Our approach is based on a one-electron model and the semi-classical approach to describe the relative motion of the two cores or nuclei. We used the straight-line constant velocity approximation, *i.e.* the internuclear distance $\mathbf{R} = \mathbf{b}+\mathbf{v}t$ with b and v respectively the impact parameter and relative velocity. This is a very accurate model for the present doubly-charged ion-atom collision systems in the range of impact energy considered (0.5–10 keV/u). The time-dependent Schrödinger equation for the electronic Hamiltonian,

$$H_{\rm e} = -\frac{1}{2}\Delta + V^{\rm t}(r) + V^{\rm p}(|\mathbf{r}-\mathbf{R}(t)|), \qquad (2.1)$$

is solved using an atomic state expansion of the wavefunction,

$$\Psi(\mathbf{r},t) = \sum_{j=1}^{N_{\rm t}} c_j^{\rm T}(t)\varphi_j^{\rm T}(\mathbf{r})\mathrm{e}^{-\mathrm{i}\varepsilon_j^{\rm T}t} + \sum_{j=1}^{N_{\rm p}} c_j^{\rm P}(t)\varphi_j^{\rm P}(\mathbf{r}-\mathbf{R})\mathrm{e}^{\mathrm{i}\mathbf{v}.\mathbf{r}}\ \mathrm{e}^{-\mathrm{i}(\varepsilon_j^{\rm P}+\frac{1}{2}v^2)t}. \qquad (2.2)$$

Here the functions $\varphi^{\rm T}$ ($\varphi^{\rm P}$) are either eigenfunctions of the isolated target (projectile) Hamiltonian or obtained by diagonalisation of these atomic Hamiltonians on a basis of, for example, Slater-type orbitals. As mentioned in the introduction, the extra factors augmenting the projectile orbitals are the Electron Translational Factors (ETF) which insure the Galilean invariance of the results[1]. The $c_j(t)$ coefficients are obtained by solving numerically a set of first-order differential coupled equations with given initial state before the collision, in the present case Li($2s$). Note that, although these coefficients can only be interpreted as probability amplitudes before and after the collision, the norm of the Ψ function (2.2) is conserved during the collision and is a reliable probe of the numerical precision in the computations.

For the two non-Coulombic atomic systems under consideration, Li(nl) and C^+(nl), we have chosen approximated frozen-core potentials to represent the core-electron interaction

$$V(r) = -\frac{1}{r}\left[Z_\infty + (Z-Z_\infty)(1+\frac{\alpha}{2}\ r)\mathrm{e}^{-\alpha r}\right] \qquad (2.3)$$

with α fixed to match the experimental binding energy of the respective ground states. The different parameters for Li and C^+ are listed in Table 1. To obtain the states for Li, He^+ and C^+, we have diagonalised the respective atomic Hamiltonians with the basis sets of Slater-type orbitals listed in Table 2.

These sets have been chosen minimal to give a good description of the important states involved in the mechanisms which give rise to excitation. This applies to the separated atom limits (*cf.* Tab. 3) and at intermediate internuclear distances, *i.e.* to the related molecular energy curves. For He^+ we have 14 states corresponding to the $1s, 2s, 2p, 3s, 3p, 3d$ sub-shells exactly described since derived from the exact Slater-type orbitals. For Li atom we have 8 states corresponding to the $2s, 2p, 3s, 3p$ sub-shells for which our one-electron model is very satisfactory,

Table 1. The parameters in the potentials to model the electron-core interaction for Li and C^+.

	Z	Z_∞	α
Li	3	1	3.31
C^+	6	2	2.83

Table 2. The radial part $(r^{n_i}\mathrm{e}^{-\lambda_i r})$ of the Slater-type orbitals used to construct the atomic s-, p- and d-states of Li, He^+ and C^+.

Li				He^+				C^+			
ℓ	i	n_i	λ_i	ℓ	i	n_i	λ_i	ℓ	i	n_i	λ_i
0	1	1	0.66055	0	1	0	2.00000	0	1	0	4.4
0	2	0	2.47673	0	2	0	1.00000	0	2	0	1.4
0	3	1	0.3835	0	3	1	1.00000	0	3	1	1.5
1	1	1	0.518	0	4	0	0.66667	0	4	2	0.8542
1	2	2	0.338	0	5	1	0.66667	0	5	3	0.59
1	3	1	1.500	0	6	2	0.66667	1	1	1	3.00
				1	1	1	1.00000	1	2	1	1.34
				1	2	1	0.66667	1	3	2	0.77
				1	3	2	0.66667	1	4	3	0.56
				2	1	2	0.66667	2	1	2	2.100
								2	2	2	0.682
								2	3	3	0.509

[1] For simplicity we assume the target fixed at the origin of the reference frame. This does not affect the generality of the equations.

Table 3. The energies (a.u.) of the states used in the present calculations obtained by diagonalising the Li, He^+ and C^+ Hamiltonians on the Slater-type orbitals basis sets listed in Table 2.

	Li		He^+		C^+
ℓ	energies	ℓ	energies	ℓ	energies
0	−1.9025788975124	0	−1.9999999998288	0	−12.277146113344
0	−0.1978449340796	0	−0.5000000001670	0	−1.2002023814554
1	−0.1298565872332	1	−0.5000000000000	1	−0.8950859767185
0	−0.0674156162289	0	−0.2222222222527	0	−0.3625824435348
1	−0.0565516863249	1	−0.2222222222222	1	−0.2997949522883
		2	−0.2222222222222	2	−0.2258437484296
				0	−0.1774898004971
				1	−0.1545888112867
				2	−0.1260159123935

especially for the 2ℓ states. For the $C^+(n\ell)$ states, our one-electron approximation is of course more questionable. The model potential in equation (2.3) (see also Tab. 1) was optimised to get correct energy for the electronic configuration $1s^2 2s^2 2p^1\ ^2$P so that we got by diagonalisation 21 states corresponding to the configurations $1s^2 2s^2 n\ell^1\ ^2$L with $n\ell = 2p, 3s, 3p, 3d, 4s, 4p, 4d$. Their energies (Tab. 3) agree well with experimental data. However, in between these different states, there exist other doublet states corresponding to the configurations:

1. $1s^2 2s^1 2p^2$, below the $1s^2 2s^2 3s^1\ ^2$S state, and with no direct importance for the excitation process under consideration;
2. $1s^2 2p^3$ whose ^{2}D state is located between the $1s^2 2s^2 3d^1\ ^2$D and $1s^2 2s^2 4s^1\ ^2$S states.

The lack of this latter one will be discussed in the Section 3.2.

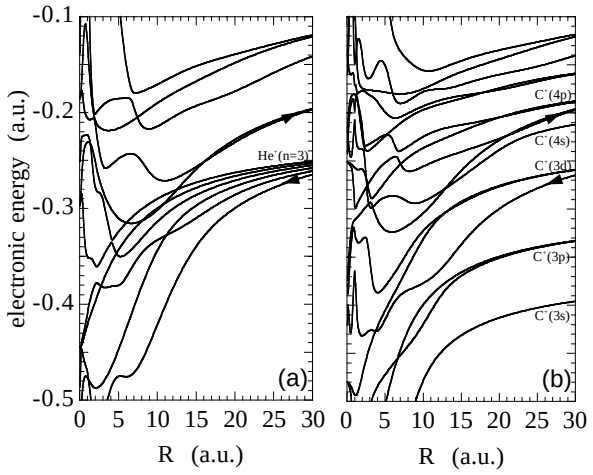

Fig. 1. Adiabatic potential energy curves of the Σ and Π states for (a) $(LiHe)^{2+}$ and (b) $(LiC)^{2+}$ collision systems. The arrows show the incoming Li($2s$) and outgoing Li($2p$) channels. The curves correlated at infinity to important capture states are labelled. The deep bound states are not shown for clarity.

2.2 The diagonalisation of the electronic Hamiltonian

The analysis of the molecular energy curves and their series of avoided crossings may be of interest to exhibit the different mechanisms responsible of the excitation. We have diagonalised the full electronic Hamiltonian of equation (2.1) onto the basis of (travelling) atomic orbitals used in the close-coupling model, *i.e.*

$$\Phi(\mathbf{r}; R) = \sum_{j=1}^{N_t} c_j^T(R)\varphi_j^T(\mathbf{r}) + \sum_{j=1}^{N_p} c_j^P(R)\varphi_j^P(\mathbf{r}-\mathbf{R})\ e^{i\mathbf{v}.\mathbf{r}}. \tag{2.4}$$

In this LCAO-type expansion note that we have kept the dynamical phase factor on the projectile orbitals for a special purpose presented in the following. This expansion is of course correct and equivalent to the adiabatic representation when the velocity is set to zero. Therefore it is only in this limit that the two-centre energy curves may be named adiabatic molecular potential energy curves. In Figure 1 we present the corresponding energy diagrams for the two collision systems, $(LiHe)^{2+}$ and $(LiC)^{2+}$. They clearly present quite different patterns, the structure of $(LiHe)^{2+}$ being much simpler due to the Coulombic ℓ-degeneracy of the He^+ states.

For non-vanishing velocities, we have to neglect some spurious dipolar couplings proportional to the velocity modulus and stemming from the ETF[2]. In this case, the diagonalisation process is therefore not strictly speaking correct and restricted to the low velocity range. A simple probe of the validity of this approximation for a given impact velocity is given by the analysis of the norm conservation of the time-dependent wavefunction (Eq. (2.2)) when projecting onto these molecular orbitals (2.4). For velocities below 0.4 a.u. (4 keV/u impact energy), we have

[2] In the diagonalisation process the choice of the origin of the reference frame (on target, projectile or for example their center of mass) is important when considering the kinetic energy term related to the ETF. For that purpose we have chosen not to include this trivial term in the energies in order to keep their values as in the separated-atom limit.

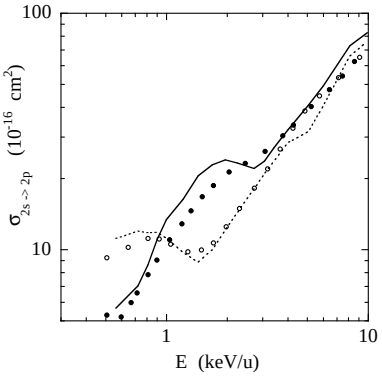

Fig. 2. Cross-sections for Li($2s \rightarrow 2p$) excitation induced by He^{2+} impact (solid line: present results) and by C^{2+} impact (dashed line: present results). The large basis close-coupling results of Brandenburg *et al.* (1998) are shown for comparison: (•) for He^{2+} impact and (○) for C^{2+} impact.

observed small departure (few percent) from unity only at small internuclear distances of no importance for the identification of the important mechanisms.

As in the adiabatic picture, one may present these pseudo energies as in the usual adiabatic diagram. These curves are then not describing the electronic structure of a transient molecule but illustrate, after the LCAO folding, the velocity-dependent couplings present in the coupled-channel calculations and responsible for the active inelastic processes. The diagrams drawn for increasing velocities will gradually present diabatic behaviours, since the ETF tend to reduce the values of the two-centre matrix elements, *cf.* discussion and Figure 4 in Section 3.2.

Finally note that the core orbitals (*cf.* Tab. 3) obtained by the diagonalisation of the isolated atom Hamiltonians were included in both the close-coupling and LCAO basis sets to get rid of spurious potential curves and unphysical couplings, see *e.g.* [11].

3 Results

3.1 The close-coupling results

Figure 2 shows the Li($2s \rightarrow 2p$) excitation cross-sections as a function of impact energy together with the results of Brandenburg *et al.* [9] performed with an extended atomic orbital basis set. The agreement between the two calculations is very good, especially in the low-energy regime where higher target states not included in our minimal basis are not important. The data of Brandenburg *et al.*, corrected by cascade contribution, were found to compare well with different experimental Li($2p \rightarrow 2s$) emission cross-sections [9]. This validates our approach.

Our results show clearly the striking differences in the behaviour of the cross-sections for the two doubly-charged collision systems:

1. for He^{2+} impact, the excitation cross-section increases monotonously except for a shoulder around 1.5 keV/u, somewhat magnified by the present model;

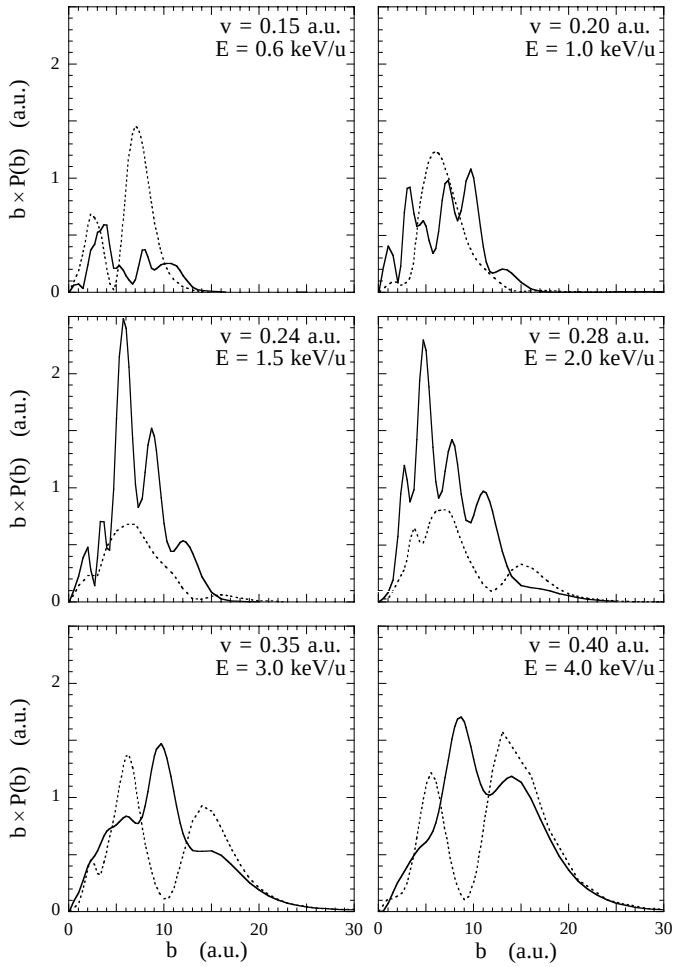

Fig. 3. Reduced probability $b \times P(b)$ for total Li($2p$) excitation as function of impact parameter b (a.u.) for six different velocities. Solid line: He^{2+} impact, dashed line: C^{2+} impact.

2. for C^{2+} impact, a secondary peak appears around 0.8 keV/u, forming a plateau from 0.5 to 2 keV/u where the cross-sections is nearly constant at about 10^{-15} cm^2.

As remarked in [9] the two different low-energy structures in these similar systems should be interpreted by the different characteristics of the transient molecules. The (non-)Coulombic features of the two projectiles and their influences are discussed in the next section.

3.2 Interpretation

In Figure 3 we present the Li($2s \rightarrow 2p$) reduced probability for different velocities covering the plateau range of the two collision systems (0.6–4.0 keV/u). Note that these quantities are those which give after integration the cross-sections presented in Figure 2.

First, for both systems, one clearly observes the interplay of the two mechanisms responsible for excitation. At low velocity the impact parameter dependent probabilities display one or several peaks around 8 a.u. while a second

clear structure develops around 15 a.u. and extends up to 30 a.u. for increasing velocities. The large impact parameter structure is the aforementioned direct process which is the main contribution to the cross-sections above 4 keV/u. On the other hand, for energies below 1 keV/u, the only contribution to the cross-sections stems from small internuclear distance molecular-typed processes. In between both mechanisms contribute to the formation of a valley, a plateau or only a shoulder depending on the system dependent separation in energy of the two processes [4].

The different energy dependences of the cross-sections for the two systems are seen to originate from the impact parameter region of 1–10 a.u. Indeed, for C^{2+} impact, the integrated probability in this region does not change significantly for velocities between 0.15 and 0.4 a.u. This gives rise to the plateau up to 2 keV/u, beyond which the large impact parameter peak starts to dominate the cross-section. For He^{2+} impact, on the other hand, the probabilities change dramatically from small values to a large oscillatory structure between 1 and 2 keV/u. The direct excitation mechanism at large impact parameters starts to increase at energies where the small impact parameter oscillations are still strong. Thus only a weak shoulder in the cross-section is seen at about 2 keV/u.

To understand these differences, we propose to analyse the active couplings in terms of velocity-dependent energy diagrams obtained by the procedure described in Section 2.2. Figure 4 presents these curves for both systems and for two selected velocities spanning the plateau regime. Note that the two upper graphs illustrate the low velocity range ($v = 0.15$ a.u.) and are quite similar to the molecular energy curves of Figure 1, demonstrating weak effects of the ETF in the two-center matrix elements.

For He^{2+} impact, the inelastic processes can only be initiated through the avoided crossing around 5 a.u. between the curve correlated asymptotically to the initial Li($2s$) state and a curve ending into the $He^+(n = 3)$ manifold. Excitation to Li($2p$) thus requires a transition at 5 a.u. followed by transitions at larger internuclear distances, typically 10 a.u. At low velocities the latter transitions are not likely, since the curves correlated to the Li($2p$) states do not penetrate fully into the curves correlated to the $He^+(n = 3)$ states. This results in small excitation probabilities, as seen for example for $v = 0.15$ a.u. in Figure 3. For a higher velocity the diagram at $v = 0.35$ a.u. in Figure 4 illustrates the effects of the ETF onto the important active couplings. Indeed a stronger diabatic behaviour is seen to develop at small internuclear distances for the curve correlated to the initial Li($2s$) state. This allows possible promotions to higher states through the region around 5 a.u. Therefore this effect strongly increases excitation against $He^+(n = 3)$ capture until the considered molecular mechanism gets less effective. Then, the direct process takes over, giving rise to the shoulder around 1.5 keV/u.

We note that our model magnify significantly the shoulder observed in experiments and verified by a similar but extended close-coupling calculation [9]. The capture $He^+(n = 4)$ states not included in our calculations and

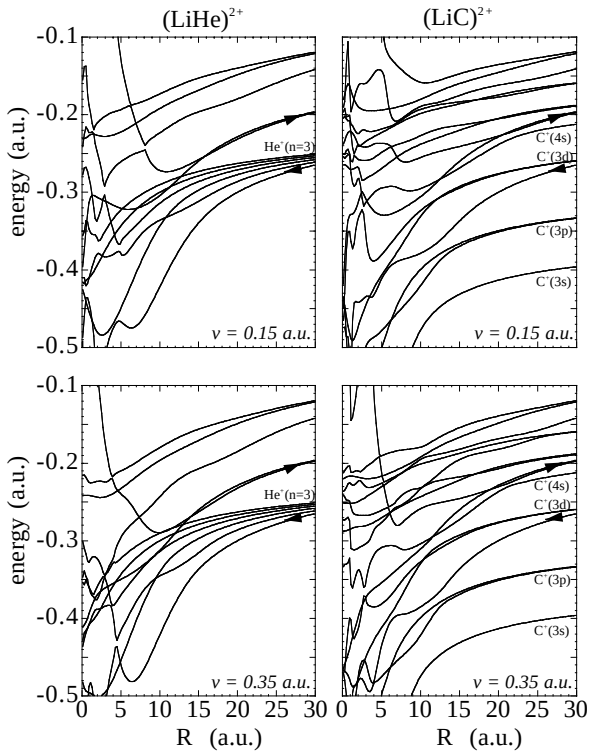

Fig. 4. Energy diagrams for the Σ and Π symmetries at velocities $v = 0.15$ and 0.35 a.u.: $(LiHe)^{2+}$, left column, and $(LiC)^{2+}$, right column. They are the results of the diagonalisation of the electronic Hamiltonian with the v-modified LCAO as presented in Section 2.2. The arrows and labels have the same meanings as in Figure 1.

present in [9] are responsible for this overestimation, *cf.* Schweinzer *et al.* [12].

For C^{2+} impact, the right panels of Figures 1 and 4 reveal a very different quasimolecular scenario compared to the other system, due to the non-degeneracy of the $C^+(n = 3)$ states. Several distinct avoided crossings involve both curves correlated asymptotically to the Li($2s$) and Li($2p$) states. Therefore an intricate competition between excitation and capture to $C^+(3\ell)$ and $C^+(4s)$ states develops for varying velocity. However, in opposition to the $(LiHe)^{2+}$ system, no clear and important changes affect the energy diagram for increasing velocities. The important crossings responsible for the molecular mechanisms leading to excitation are hardly modified by the ETF included in the calculations, *cf.* for example the avoided crossing at about 5 a.u. involving the initial channel (Fig. 4). Therefore for velocities below 0.35 a.u. no spectacular changes are expected in the excitation probabilities, as shown in Figure 3. This results in the plateau observed for that system before the direct mechanism starts to work, *cf.* Figure 1.

Finally, as mentioned in Section 2.1, our model for C^+ states does not take into account doublet states of the electronic configurations $1s^2 2s^1 2p^2$ and $1s^2 2p^3$. The former ones, located below $C^+(3s)$, clearly cannot be of any importance in the description of Li($2p$) excitation, and would

only slightly modify the $C^+(3s)$ capture results. The ^2D state of the latter ones is just above $1s^2 2s^2 3d^1$ and may have some influence at low velocities. Indeed the addition of extra curves connected to this state may significantly lower the curves correlated asymptotically to $C^+(3d)$. For velocities below 0.15–0.20 a.u. (*cf.* Fig. 4), this effect could somewhat promote $C^+(3d)$ capture and therefore slightly decreases our results for excitation.

4 Conclusion

In this paper we have performed a study of the dynamics behind a striking difference in the cross-sections for $Li(2s \rightarrow 2p)$ excitation by He^{2+} and C^{2+} projectiles. The different plateau structures are described and interpreted successfully by the present minimal atomic-state close-coupling approach. It is explicitly shown how the structures in the cross-sections originate from two mechanisms as previously demonstrated in model calculations [4]: a low energy molecular-typed one and an intermediate energy direct one. The existence of the plateaus for the two collision systems are then interpreted by the analysis of the important ETF-modified couplings illustrated with velocity dependent energy diagrams.

The large scale computations have been performed at Institut du Développement et des Ressources en Informatiques Scientifiques (IDRIS) and at Norwegian super computing facilities through a TRU grant. The research has been supported by the Bergen Computational Physics Laboratory (BCPL) under EU contract HPRI-1999-000161.

References

1. K.B. MacAdam, J.C. Day, J.C. Aguilar, D.M. Homan, A.D. MacKellar, M.J. Cavagnero, Phys. Rev. Lett. **75**, 1723 (1995).
2. D.R. Schultz, C.O. Reinhold, P.S. Krstić, Phys. Rev. Lett. **78**, 2720 (1997).
3. W. Fritsch, C.D. Lin, Phys. Rev. A **26**, 762 (1982).
4. J.P. Hansen, L. Kocbach, S.A. Synnes, J.B. Wang, A. Dubois, Phys. Rev. A **57**, R4086 (1998).
5. P.S. Krstić, C.O. Reinhold, D.R. Schultz, J. Phys. B: At. Mol. Opt. Phys. **31**, L155 (1998).
6. D.R. Bates, R. McCarroll, Proc. R. Soc. A **245**, 175 (1958).
7. D. Dowek, J.C. Houver, I. Reiser, J. Salgado, A. Svensson, J.W. Thomsen, N. Andersen, S.E. Nielsen, A. Dubois, Phys. Rev. A **54**, 970 (1996).
8. J. Salgado, J.W. Thomsen, N. Andersen, D. Dowek, A. Dubois, J.C. Houver, S.E. Nielsen, I. Reiser, A. Svensson, J. Phys. B: At. Mol. Opt. Phys. **30**, 3059 (1997).
9. R. Brandenburg, J. Schweinzer, F. Aumayr, H.P. Winter, J. Phys. B: At. Mol. Opt. Phys. **31**, 2585 (1998).
10. J.W. Turkstra, D. Meyer, R. Hoekstra, R. Morgenstern, J. Schweinzer, Phys. Rev. A **60**, 4627 (1999).
11. N. Toshima, J. Phys. B: At. Mol. Opt. Phys. **27**, L49 (1994).
12. J. Schweinzer, D. Wutte, H.P. Winter, J. Phys. B: At. Mol. Opt. Phys. **27**, 137 (1994).